
TOWARD ACCURATE RUL AND SOH ESTIMATION USING REINFORCED GRAPH-BASED PINNS ENHANCED WITH DYNAMIC WEIGHTS

Mohamadreza Akbari Pour

Department of Mechanical Engineering
Sharif University of Technology
Teymouri Square, Tarasht, Tehran, Iran
mohamadreza.akbari83@sharif.edu

Ali Ghasemzadeh

Department of Computer Engineering
Sharif University of Technology
P.O. Box 11155-9517
ali.ghasem01@sharif.edu

Mohamad Ali Bijarchi

Department of Mechanical Engineering
Sharif University of Technology
Teymouri Square, Tarasht, Tehran, Iran
bijarchi@sharif.edu

Mohammad Behshad Shafii

Department of Mechanical Engineering
Sharif University of Technology
Teymouri Square, Tarasht, Tehran, Iran
behshad@sharif.edu

July 15, 2025

ABSTRACT

Accurate estimation of Remaining Useful Life (RUL) and State of Health (SOH) is essential for Prognostics and Health Management (PHM) across a wide range of industrial applications. We propose a novel framework—Reinforced Graph-Based Physics-Informed Neural Networks Enhanced with Dynamic Weights (RGPD)—that combines physics-based supervision with advanced spatio-temporal learning. Graph Convolutional Recurrent Networks (GCRNs) embed graph-convolutional filters within recurrent units to capture how node representations evolve over time. Graph Attention Convolution (GATConv) leverages a self-attention mechanism to compute learnable, edge-wise attention coefficients, dynamically weighting neighbor contributions for adaptive spatial aggregation. A Soft Actor-Critic (SAC) module is positioned between the Temporal Attention Unit (TAU) and GCRN to further improve the spatio-temporal learning. This module improves attention and prediction accuracy by dynamically scaling hidden representations to minimize noise and highlight informative features. To identify the most relevant physical constraints in each area, Q-learning agents dynamically assign weights to physics-informed loss terms, improving generalization across real-time industrial systems and reducing the need for manual tuning. In both RUL and SOH estimation tasks, the proposed method consistently outperforms state-of-the-art models, demonstrating strong robustness and predictive accuracy across varied degradation patterns across three diverse industrial benchmark datasets.

1 Introduction

Prognostics and Health Management (PHM) has become a cornerstone of efficiency, cost reduction, and operational reliability in today's rapidly evolving industrial landscape [1]. Remaining Useful Life (RUL) and State of Health (SOH) are two crucial metrics in this field that are essential for maximizing asset performance, reducing downtime, and improving safety [2]. RUL is the time before a machine or component breaks down or needs maintenance, whereas SOH reflects the current condition of the system relative to its optimal or original state [3]. The accurate estimation of RUL and SOH in industrial systems stands as a central objective within the PHM applications. By leveraging data-driven approaches and advanced analytical techniques, PHM frameworks aim to forecast the degradation and potential failure of a broad spectrum of sophisticated machinery and equipment [4].

PHM frameworks are designed to predict the deterioration and eventual failure of a wide range of complex machinery and equipment by utilizing data-driven methodologies and cutting-edge analytical techniques. This capability holds immense practical value across numerous industrial domains, facilitates a shift toward proactive maintenance practices, and enhances system reliability [5]. Consequently, it contributes significantly to financial and operational improvements. Prediction efforts primarily fall into three main categories: physical model-based methods, which depend on knowledge of underlying degradation mechanisms; data-driven methods, which leverage historical data to develop predictive models; and hybrid methods, which integrate the strengths of both approaches [6].

In physical model-based methods, RUL and SOH estimation hinge on a thorough understanding of the equipment's underlying degradation mechanisms and operational principles [7]. These approaches often involve establishing mathematical models that describe the physical processes, which leads to failure. Many methods rely on understanding degradation mechanisms and evolution patterns, as well as specific models include particle filters for damage prognosis [8] and Bayesian filtering approaches [9] that accounts for different failure mechanisms.

Some studies even incorporate modified physical laws like Paris's law to predict damage propagation [10]. Conversely, data-driven methods use historical condition monitoring data to train algorithms in order to predict RUL without requiring explicit knowledge of the physical degradation processes. With the rapid advancement of deep learning, various neural network architectures have demonstrated significant potential in this area. These include Recurrent Neural Networks (RNNs) [11] and their variants like Long Short-Term Memory (LSTM) [12] and Gated Recurrent Units (GRUs) [13], Convolutional Neural Networks (CNNs) [14], and Graph Neural Networks (GNNs) [15].

In order to more precisely estimate RUL and SOH, these models learn complex temporal and spatial dependencies from data. By creating graph-structured data with input channels acting as nodes and their relationships as edges, GNNs in particular are excellent at capturing spatial correlations between multiple input channels.

For instance, when aggregating information for each node, Graph Attention Networks (GATs) [16] use attention mechanisms to balance the importance of various neighboring nodes. Other GNN-based methods combine temporal models such as RNNs or LSTMs with graph convolutions like graph convolutional networks (GCNs) [16], which integrate graph convolutions with gated recurrent units, to simultaneously extract spatio-temporal dependencies.

However, these approaches often require substantial amounts of data for effective training, and their prediction accuracy can be compromised if the characteristics of test data differs significantly from the one used for training. Furthermore, purely data-driven models can be perceived as "black boxes" due to lack of transparency and interpretability and this is a critical concern in safety-critical industrial applications [17]. These models may not always follow basic physical principles when there are no explicit physical constraints [18]. Deep learning architectures often suffer from overfitting and an increase in parameters as they become more complex in an attempt to achieve higher accuracy. This might hinder their deployment and real-time inference. Moreover, a significant drawback is that data-driven methods might not be able to effectively utilize any prior knowledge that might be available about the system's degradation. Additionally, certain data-driven approaches might process spatial and temporal features in isolation and potentially overlook crucial interdependencies between them .

Collectively, hybrid methods aim to capitalize on the strengths of both physical and data-driven approaches, and they integrate them to enhance prediction accuracy and reliability. Hybrid approaches can provide a more thorough understanding of system degradation by fusing the interpretability of physical models with the learning potential of data-driven methodologies. Within this paradigm, the synergistic combination of different neural network architectures with physics-informed models is gaining increasing attention. For example, Physics-Informed Neural Networks (PINNs) [19] are a powerful class of hybrid models in which the training process of neural networks incorporates physical laws or governing equations to regularize learning and enhance the physical consistency of the predictions of system degradation.

Furthermore, other hybrid methodologies integrate statistical models with data-driven ones, such as the combination of a particle filter (PF) with an autoregressive integrated moving average (ARIMA) model (PF-ARIMA) to account for capacity regeneration phenomena in lithium-ion batteries [20]. A promising path in the creation of sophisticated hybrid models for RUL and SOH estimation is highlighted by the tendency to combine physics-based principles with the special strengths of various deep learning architectures.

Although these models perform well, achieving higher accuracy and generalization often requires extensive hyperparameter tuning, which is impractical in industrial settings. Additionally, the relative importance of different loss terms or physical laws in PINNs can vary across datasets due to factors such as noise introduced by measurement errors. Therefore, dynamically adapting the weights assigned to each physical constraint can help address these challenges and improve model robustness.

Reinforcement Learning is a powerful AI approach that combines trial-and-error learning with search and optimization to solve complex decision-making problems. When paired with deep learning, it is much more effective and allows for superhuman performance on a variety of tasks [21]. Since RL can explore and generalize through search strategies, it performs exceptionally well on control tasks. The application of DRL is evident in several industrial contexts [22]. Furthermore, a system-centered PHM re-optimization method utilizing multi-agent DRL has been proposed to address the complexities of multi-component systems, where collaborative learning among agents facilitates phased decision-making [23]. DRL has also been explored for fatigue life prognosis of composite structures, with the integration of transfer learning to enhance generalizability in data-scarce scenarios [24]. It should be noted that DRL algorithms often require extensive computational resources and large amounts of data to train effectively, and this leads to issues with stability and convergence that are not simply solved. For actual industrial applications where resources and data may be scarce, it renders them less feasible. Using a simple RL model like Q-learning is suitable for this task, as finding appropriate weights isn't overly complex and doesn't require a powerful RL algorithm. Furthermore, Q-learning usually converges quickly, that makes the approach more practical and easier to implement.

To cope with the mentioned challenges, we propose a comprehensive framework to estimate SOH and RUL as crucial system health indicators, By combining the benefits of GNNs and TAU, together with the physical definition of the RUL prediction that is empowered by RL agents. An overview of the framework is sketched in Figure 1. The main contributions of this work are summarized as follows:

- We propose a novel spatio-temporal graph neural network that integrates Graph Attention Convolutional Networks (GATConv), Graph Convolutional Recurrent Networks (GCRN), and a Temporal Attention Unit (TAU) to estimate (RUL) and (SOH) in complex systems. By constructing a well-defined adjacency matrix, input data is organized into a graph structure that captures system degradation patterns. GATConv adaptively assigns weights to input channel nodes, effectively modeling spatial dependencies, while GCRN captures temporal dynamics within the transformed data. The TAU further enhances the model's ability to learn intricate spatio-temporal patterns by focusing on significant temporal features.
- This integration marks the first application of both Graph Neural Networks (GNNs) and Physics-Informed Neural Networks (PINNs) in industrial degradation modeling, establishing a new paradigm in the field. By uniquely combining these methodologies, our model enhances accuracy, reliability, and interpretability. Specifically, PINNs incorporate physical laws to ensure that model predictions align with the dynamics of real-world systems, while GNNs capture spatial and temporal dependencies in the input data. This synergistic approach not only improves predictive performance but also provides deeper insights into the degradation processes, setting a new standard for future research and applications in this domain.
- We give the physics-informed loss terms dynamic weights using Q-learning agents. Without any requirement for manual hyperparameter tuning, the agents automatically modify these weights to minimize RMSE and speed up convergence by utilizing a ϵ -greedy exploration strategy over a discretized weight space. We also employ Soft Actor-Critic (SAC) to dynamically learn a scaling factor applied to the hidden representations from the GCRN before they are passed to the Temporal Attention Unit (TAU). This adaptive scaling mitigates the influence of noisy or low-salience features, stabilizes gradient flow, and improves attention learning.
- Three different and popular datasets are used to assess our implementation: the XJTU battery dataset, which contains degradation data from 55 lithium-ion batteries; the CMAPSS dataset, a benchmark for engine prognostics with extensive lifetime data; and the PRONOSTIA bearing dataset, which offers run-to-failure data for deep-groove ball bearings. Interestingly, our model performs admirably on each of the three datasets. This highlights the generalization ability and robustness of our approach, making it suitable for diverse industrial applications. The use of the Mixup data augmentation technique further contributes to this generalizability by encouraging smoother decision boundaries and enhancing model resilience to variations in the data.

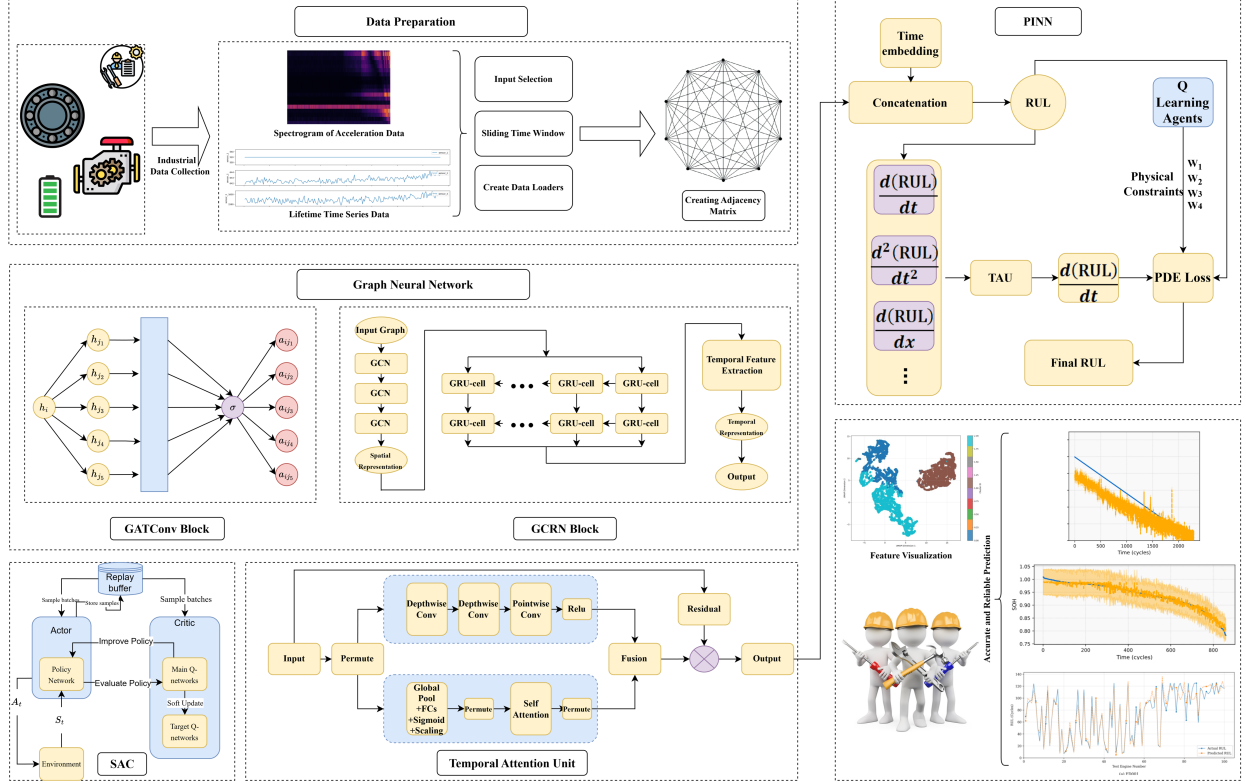


Figure 1: Overall framework of the proposed method.

2 Methodology

2.1 Temporal Attention Unit (TAU)

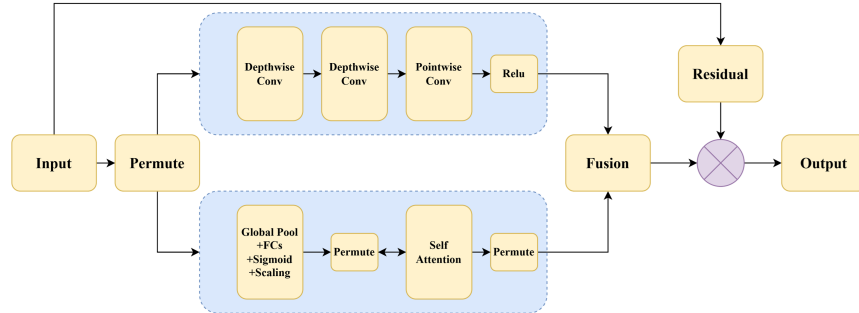


Figure 2: Temporal attention unit.

TAU is one of the sophisticated modules that can extract temporal features and focus on relevant time steps using both convolutional and attention mechanisms [25, 26], It consists of Dynamic Attention (DA using Average Pooling and a Fully connected layer), Static Attention (SA using depth-wise convolutions, dilated convolutions, 1×1 convolutions). These makes TAU really powerful to capture complicated spatio-temporal patterns, features and model long-range dependencies, it also enhances Robustness. this model works like:

$$SA = \text{Conv}_{1 \times 1}(\text{DW-D Conv}(\text{DW Conv}(H)))$$

$$DA = \text{FC}(\text{AvgPool}(H))$$

$$H' = (SA \otimes DA) \odot H$$

where H is hidden feature that is given to the TAU and \otimes is Kronecker product and \odot is Hadamard product. Figure 2 represents TAU’s detailed parameters.

2.1.1 Depthwise Convolution

It’s a type of convolution that performs a single convolution per input channel instead of mixing channels and it reduces the computational cost, and architectures like MobileNet use this to build efficient models that perform well. It is applied on an input tensor $\mathbf{X} \in \mathbb{R}^{H \times W \times C}$ (with height H , width W , and channels C) like below :

$$Y_c = X_c \times X_c, \quad \text{for } c = 1, \dots, C$$

where K_c is the kernel corresponding to channel c .

2.1.2 Dilated Convolution

It is a very powerful type of convolution introduces gaps between kernel elements, and with the same number of parameters increases the receptive field. This allows the network to capture long-short-range dependencies and multi-scale context effectively. For a 1D input signal x and a filter size k , a dilated convolution is defined as :

$$(y *_d f)(i) = \sum_{j=0}^{k-1} f(j) \cdot x(i - d \cdot j).$$

where d is dilation rate.

2.1.3 Pointwise Convolution

Pointwise convolution commonly referred to 1×1 convolution and is a fundamental operation in CNNs to utilize the process of data. It helps mix information from different channels and reduce the dimensions and make the model less complex, it also extracts good features and more abstract features and is highly used in models like MobileNet that require efficiency and generalization. This convolution applies on input tensor X with C channels, and a kernel $K \in \mathbb{R}^{1 \times 1 \times C \times C'}$ pointwise convolution is defined as :

$$Y(i, j, c') = \sum_{c=1}^C X(i, j, c) \cdot K(1, 1, c, c').$$

2.1.4 Multi-Head Self-Attention

Self-Attention mechanism which is widely used in natural language processing for assigning levels of importance to different elements of a sequence is a powerful model on time series and can improve the predictions. In multi-head self-attention, the model can focus on different parts of the input simultaneously, and captures diverse relationships and long-range dependencies. This applies to an input X and extracts queries Q , keys K , and values V using linear transformations. Then, attention is defined as:

$$\text{Attention}(Q, K, V) = \text{softmax}\left(\frac{QK^T}{\sqrt{d_k}}\right)V$$

where the d_k is the dimension of queries and keys. In multi-head attention, this process is executed in parallel multiple times, and results are concatenated to form the final output.

2.2 Graph Convolutional Recurrent Neural Network (GCRN)

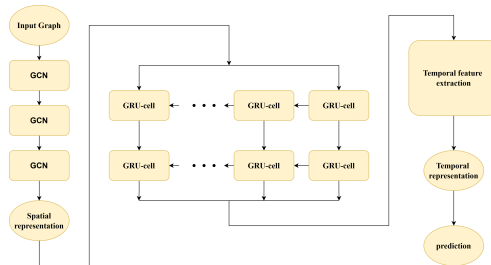


Figure 3: GCRN block.

Traditional recurrent neural networks(RNNs), are very good at extracting and learning features on sequential data like time series and can be effective for predicting Remaining Useful Life(RUL), there are also graph convolutional networks (GCNs) and they are good at capturing spatial dependencies in graph-structured data, so when we combine these two architectures we can model both spatial and temporal dependencies efficiently. So first we review Graph Convolutional Network and Gated Recurrent Unit which build the GCRN shown in Figure 3:

2.2.1 Graph Convolutional Networks

GCNs [27] are an extension of the convolution for graph-structured data and performs message passing between neighboring nodes and can capture local structural information. Mathematically a GCN operation is defined by:signals for remaining useful life prediction

$$H^{l+1} = \sigma(\tilde{D}^{-\frac{1}{2}} \tilde{A} \tilde{D}^{-\frac{1}{2}} H^{(l)} W^{(l)})$$

where \tilde{A} is the adjacency matrix of the undirected graph with self-loops, and $\tilde{D}_{ii} = \sum_j \tilde{A}_{ij}$

2.2.2 Graph Attention Convolution Network

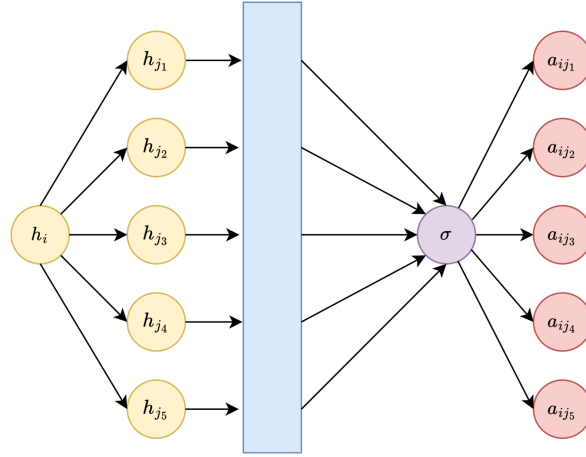


Figure 4: graph attention convolution network.

GAT is based on the idea that not all connections are equally important. It assigns different attention scores to different neighbors and allows the model to focus on the most relevant relationships, each node has features that are first transformed using a learnable weight matrix W . It uses an attention function to decide the importance of each neighbor, computed as :

$$e_{i,j} = \text{LeakyReLU}(a^T [Wh_i || Wh_j])$$

then applies softmax normalization to convert them to attention weights:

$$a_{ij} = \frac{\exp(e_{ij})}{\sum_k \exp(e_{ik})}$$

each node then aggregates the features of its neighbors, weighted by the attention scores :

$$h'_i = \sigma \left(\sum_j a_{ij} Wh_j \right)$$

The output of the GAT layer with multi-head attention is :

$$h_i^{(l+1)} = \sigma \left(\frac{1}{K} \sum_{k=1}^K \sum_{j \in N_i} a_{ij}^k W^k h_j^{(l)} \right)$$

and the K is the number of attention heads.

As shown in Figure 4, The GATConv layer, widely used in Graph Attention Networks, formalizes the attention-based message passing mechanism by computing node embeddings as weighted aggregations of their neighbors. Specifically, each node i updates its representation by attending to features of neighboring nodes $j \in \mathcal{N}(i)$ using learned attention coefficients α_{ij} :

$$\mathbf{h}'_i = \sum_{j \in \mathcal{N}(i)} \alpha_{ij} W \mathbf{h}_j.$$

2.2.3 Gated Recurrent Unit (GRU)

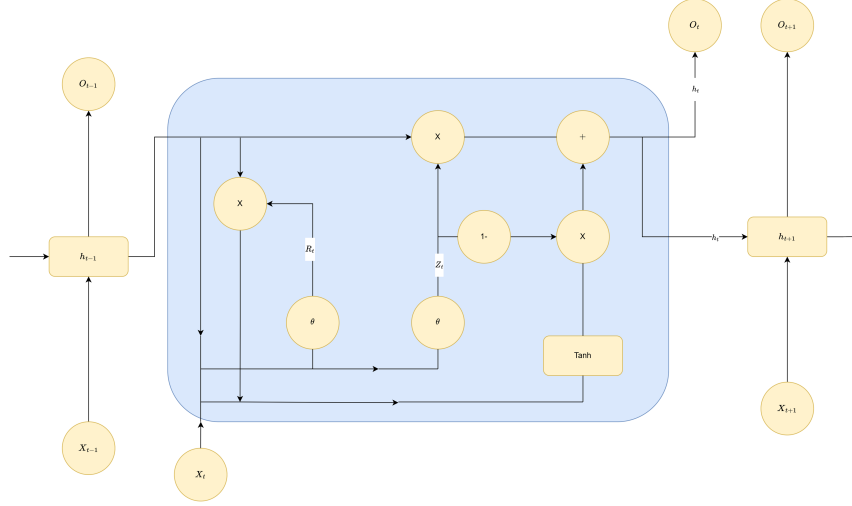


Figure 5: gated recurrent unit.

After extracting spatial features from the graph, a recurrent network models the temporal dependencies. The Gated Recurrent Unit (GRU) [28], shown in Figure 5, is an RNN that can handle the long-term dependencies efficiently. A GRU is defined by:

$$\begin{aligned} z_t &= \sigma(W_z x_t + U_z h_{t-1}) \\ r_t &= \sigma(W_r x_t + U_r h_{t-1}) \\ \tilde{h}_t &= \tanh(W_h x_t + r_t \odot (U_h h_{t-1})) \\ h_t &= (1 - z_t) \odot h_{t-1} + z_t \odot \tilde{h}_t \end{aligned}$$

where x_t is the input, h_t is the output, z_t is the update gate vector, r_t is the reset gate.

2.3 Deep Hidden Physics Models (DeepHPM)

DeepHPM [29] is a framework that aims to discover the governing equations, and It can learn nonlinear partial differential equations(PDEs) of complex dynamical systems from the observed data by using the power of neural networks. This model uses DNNs to learn both the system's solution and the structure of its dynamics.

It consists of a Solution Network, which is a neural network that approximates the unknown solution $u(x,t)$ of the dynamical system. This network acts as a smooth function approximator.

It also consists of a Dynamics Network that approximates the nonlinear function \mathcal{N} in the governing PDE, which is often written as :

$$u_t = \mathcal{N}(t, x, u, u_x, u_{xx}, \dots)$$

This can be modeled by a DNN.

Then a deep hidden physics model f is defined :

$$f := u_t - \mathcal{N}(t, x, u, u_x, u_{xx}, \dots).$$

We take the derivatives of neural network u with respect to time t and space x using chain rule.

2.3.1 Physical constraint

The model enforces physical constraints on SOH and RUL estimation, denoted \hat{y}_t , to ensure monotonic degradation, smooth dynamics, consistency with the neural PDE, and zero RUL for failed devices or when battery SOH falls below 0.8.

- **Monotonicity:** RUL decreases over time ($\frac{d\hat{y}}{dt} \leq 0$).

$$\text{diff1} = \hat{y}_{t+1} - \hat{y}_t, \quad \text{pde_residual1} = \max(0, \text{diff1})$$

Loss: $w_1 \cdot \text{mean}(\text{pde_residual1}^2)$.

- **Smoothness:** Degradation rate changes smoothly.

$$\text{diff2} = (\hat{y}_{t+2} - \hat{y}_{t+1}) - (\hat{y}_{t+1} - \hat{y}_t)$$

Loss: $w_2 \cdot \text{mean}(\text{diff2}^2)$.

- **Neural PDE:** RUL derivative matches learned dynamics (N_u).

$$\text{residual} = \text{diff1} - N_u[:, :, -1, 0]$$

Loss: $w_3 \cdot \text{mean}(\text{residual}^2)$.

- **Failed devices:** RUL ≈ 0 or SOH ≤ 0.8 when the device has failed or SOH is below threshold.

$$\text{broken_loss} = \text{mean}(\text{broken_mask} \cdot \hat{y}_{\text{last}}^2)$$

This loss is added to the PDE loss.

Total PDE Loss

$$\begin{aligned} \text{pde_loss} = & w_1 \cdot \text{mean}(\text{pde_residual1}^2) + w_2 \cdot \text{mean}(\text{diff2}^2) \\ & + w_3 \cdot \text{mean}(\text{residual}^2) + w_4 \cdot \text{broken_loss} \end{aligned}$$

An overview of the proposed PINN structure is sketched in Figure 6.

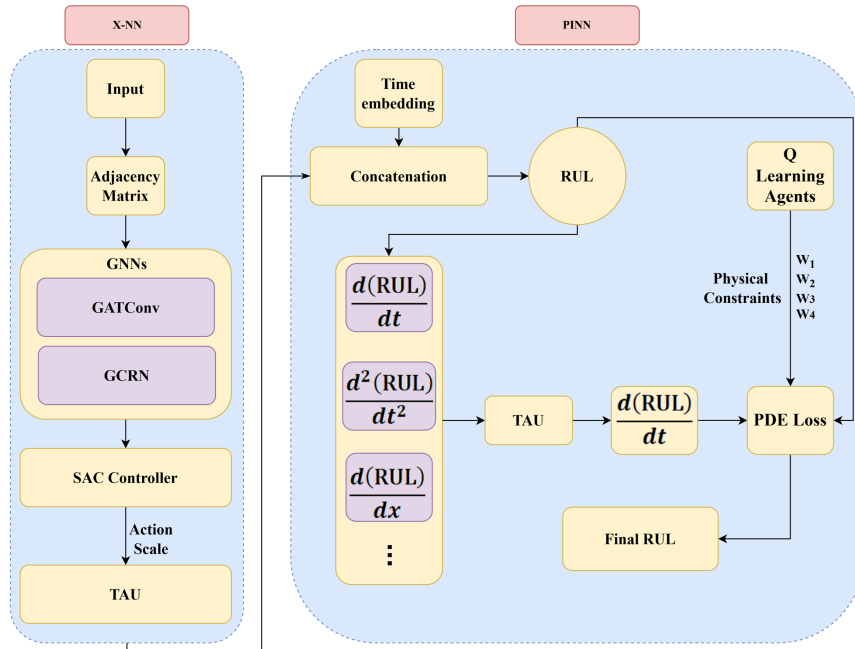


Figure 6: Proposed PINN integrated graph-based neural network.

2.4 Reinforcement Learning

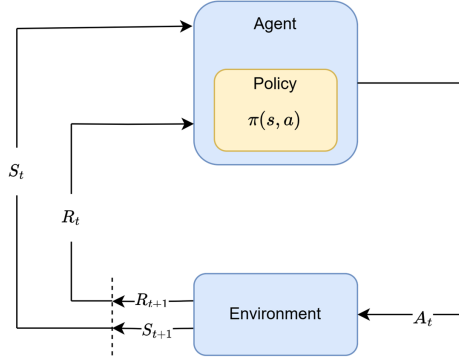


Figure 7: Reinforcement learning approach.

Figure 7 represents Reinforcement Learning, a leading subfield of AI that leverages trial-and-error interactions with an environment to learn optimal decision-making policies from feedback. In our model, we use two famous RL algorithms to control the weights of PDE loss and dynamically adjust the features extracted from the networks.

2.4.1 Q-learning

Q-learning [30] is one of the foundational algorithms in reinforcement learning. It is a model-free and off-policy, it aims to learn the optimal action-value function, denoted as $Q(s, a)$ which is the estimation of the expected cumulative reward for taking action a in state s . the update rule is :

$$Q(s_t, a_t) \leftarrow Q(s_t, a_t) + \alpha [r_{t+1} + \gamma \max_{a'} Q(s_{t+1}, a') - Q(s_t, a_t)]$$

and $Q(s_t, a_t)$ is the current estimate of Q-value and r_{t+1} is the received reward after taking action a_t in state s_t , $\max_{a'} Q(s_{t+1}, a')$ represents the estimated optimal future reward from the next state s_{t+1} .

- Agent 1 selects w_1 from a discrete action space $\{0.1, 0.5, 1.0, 2.0, 5.0, 10.0\}$ based on state $s_1 = (\text{mean}(\text{pde_residual}^2))$
- Agent 2 selects w_2 from $\{0.01, 0.05, 0.1, 0.5, 1.0, 2.0\}$ based on state $s_2 = (\text{mean}(\text{diff}^2))$.
- Agent 3 selects w_3 from $\{0.1, 0.5, 1.0, 2.0, 5.0, 10.0\}$ based on states $s_3 = \text{mean}(\text{diff}1 - N_u)^2$
- Agent 4 w_4 from $\{0.1, 0.5, 1.0, 2.0, 5.0, 10.0\}$ based on state $s_4 = \text{broken_loss}$ from
- Q-tables are updated using reward $r = 10 \cdot (\text{prev_rmse} - \text{valid_rmse})$ using ϵ -greedy exploration

Weights are based on the physics-based losses terms and are selected dynamically, eliminating need for manual hyperparameter tuning for weights. Additionally we observe that different datasets have different optimal weights. To balance trade-off between exploration and exploitation we use *epsilon*-greedy method. These agents dynamically choose different weights to to reduce the RMSE and maximize the improvement between previous and current RMSE which leads to faster convergence at each step. selecting weights from a continuous space would increase the model's complexity; therefore, we restrict the choices to discrete set of values within a bounded range. Furthermore, as the model become close to the optimal solution model can reduce the weights to prevent divergence.

2.4.2 Soft Actor-Critic (SAC)

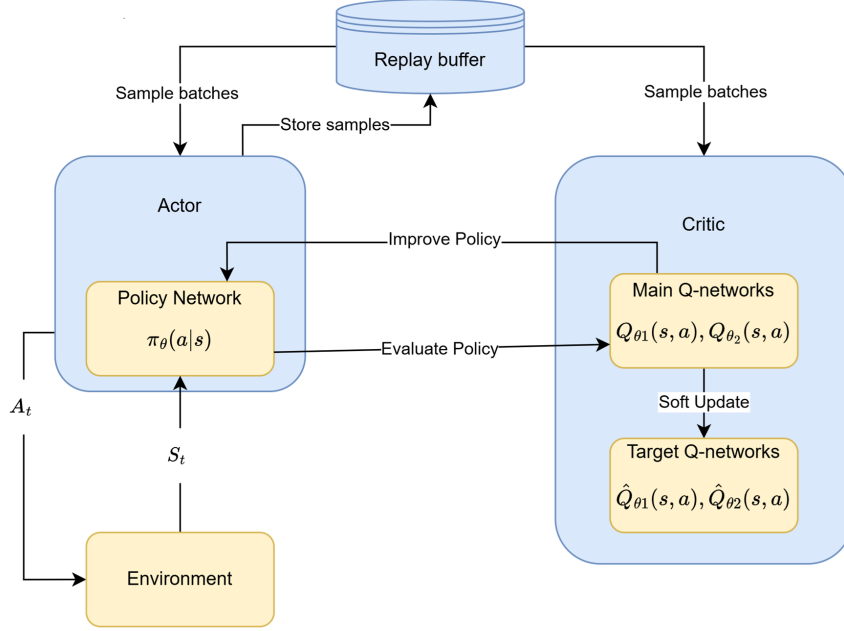


Figure 8: Soft actor critic.

Figure 8 shows SAC [31] which is one of state-of-art-policy reinforcement learning algorithms. SAC not only focuses on maximizing the expected return but also consider the diversity in actions by avoiding assigning all probability mass to a single action. In traditional reinforcement learning, the objective is :

$$J(\pi) = \mathbb{E}_\pi \left[\sum_t \gamma^t r(s_t, a_t) \right]$$

However, SAC modifies this objective by adding an entropy term weighted by a coefficient α , promoting exploration and diversity of actions :

$$J(\pi) = \mathbb{E}_\pi \left[\sum_t \gamma^t (r(s_t, a_t) + \alpha \mathcal{H}(\pi(\cdot|s_t))) \right]$$

where the $\mathcal{H}(\pi(\cdot|s_t)) = -\mathbb{E}_{a \sim \pi} [\log(\pi(a|s_t))]$ measures the randomness of the policy at state s_t , maximizing entropy encourages the policy to distribute probability mass over multiple actions rather than concentrating it on a single one. SAC also employs a modified Bellman backup operator \mathcal{T}^π defined as :

$$\mathcal{T}^\pi Q(s_t, a_t) \triangleq r(s_t, a_t) + \gamma \mathbb{E}_{s_{t+1} \sim p} [V(s_{t+1})]$$

where

$$V(s_t) = \mathbb{E}_{a_t \sim \pi} [Q(s_t, a_t) - \log \pi(a_t|s_t)]$$

and

$$\pi_{\text{new}} = \arg \min_{\pi' \in \Pi} D_{KL} \left(\pi'(\cdot|s_t) \parallel \frac{\exp(Q^{\pi_{\text{old}}}(s_t, \cdot))}{Z^{\pi_{\text{old}}}(s_t)} \right).$$

reward = -supervised_{loss} = -MSE(y_{pred} , y_{ture})

$$L_{\text{actor}} = \mathbb{E}[\alpha * \log \pi(a|s) - Q(s, a)]$$

$$L_{\text{critic}} = \text{MSE}(Q(s, a), r + \gamma(1 - d))$$

Our proposed method employs SAC to find the scaling factor for the hidden layer after GCRN and before the data is fed into the TAU block. Since some features are too noisy or have low significance for TAU, this scaling acts as a kind

of normalization step, adaptively strengthening or weakening features. SAC adaptively scales hidden-state features to an optimal range, preventing gradient instability and saturation in TAU’s attention and convolution operations. By amplifying or suppressing specific feature dimensions, SAC implicitly guides TAU to focus on physically relevant patterns. The actor-critic framework ensures smooth gradient flow into TAU by maintaining feature magnitudes within learnable bounds, unlike fixed initialization schemes.

2.5 Mixup

A common problem of the data-driven model is overfitting to the training data which leads poor performance in other domains. To mitigate overfitting, several regularization methods are used, such as dropout, l2-norm. Another effective regularization technique is Mixup [32], which generates synthetic training samples by linearly combining pairs of samples. Mixup performs well in this task because accurate prediction near end-of-life (low RUL) is crucial. By generating synthetic samples in these critical ranges, Mixup helps the model generalize better. Moreover, input channels’s features often exhibit physical interdependencies, and Mixup preserves these correlations when blending samples, making it a suitable choice for regularization in this context. The Mixup formulation for training samples $(x_i, y_i), (x_j, y_j)$ is :

$$\hat{x} = \lambda x_i + (1 - \lambda)x_j$$

$$\hat{y} = \lambda y_i + (1 - \lambda)y_j$$

where $\lambda \in [0, 1]$

2.6 Algorithm summary

We summarized the total process of training and model in the below :

Algorithm 1 Training of model.

Require: Preprocessed datasets $\{D_{train}, D_{valid}, D_{test}\}$ and configuration hyperparameters

```

1: for  $i = 1$  to  $D$  do
2:   Build DataLoaders train, val from  $D_{train}, D_{valid}$ 
3:   Construct temporal graph edge_index for window length  $|T_{train}^i|$ 
4:   Initialization  $M^i \leftarrow \text{custom}_{model}(\text{config})$ 
5:   Initialize optimizer with Xavier-uniform, scheduler
6:   for each epoch do
7:     for each batch  $(x, t, y)$  in train do
8:        $(x', y', \lambda, \cdot) \leftarrow \text{mixup\_data}(x, y, \alpha_{\text{mixup}})$ 
9:        $(\hat{y}, \mathcal{L}_{\text{PDE}}, s, a, \log p) \leftarrow M^i(x', t, \text{edge\_index}, \text{targets} = y')$ 
10:       $\mathcal{L}_{\text{sup}} \leftarrow \text{mixup\_criterion}(\hat{y}, y', y[\cdot], \lambda)$ 
11:       $\mathcal{L} \leftarrow \mathcal{L}_{\text{sup}} + w_{\text{pde}} \cdot \mathcal{L}_{\text{PDE}}$ 
12:      Backpropagate  $\mathcal{L}$ , update  $M^i$  every  $k$  steps
13:      Push  $(s, a, r = -\mathcal{L}_{\text{sup}}, s, 1.0)$  into SAC buffer
14:      Update SAC agent
15:     end for
16:   end for
17: end for

```

Algorithm 2 RGPD approach.

Require: Input features $X \in \mathbb{R}^{B \times T \times D}$, time-stamps $t \in \mathbb{R}^{B \times T}$, graph edges E , true labels $Y \in \mathbb{R}^B$

- 1: **1. Spatial-Temporal Feature Encoding**
- 2: $H \leftarrow$ apply GATConv on (X, E)
- 3: $H_G \leftarrow$ apply GCRNBOCK on (H, E)
- 4: $s \leftarrow$ mean over H_G ▷ global state for SAC
- 5: **2. SAC-Based Feature Modulation**
- 6: $(\text{action}, \log p) \leftarrow$ apply SACController on s
- 7: $H_G \leftarrow H_G \cdot (1 + \text{action})$
- 8: **3. TAUBlock & Time Embedding**
- 9: $H_T \leftarrow$ apply TAU_block on H_G
- 10: $T_{\text{emb}} \leftarrow$ apply timeEmbed on $\frac{t}{T_{\text{max}}}$
- 11: $F \leftarrow$ concat(H, T_{emb})
- 12: **4. RUL Prediction**
- 13: $\hat{Y}_{\text{seq}} \leftarrow$ Linear(F)
- 14: **if training then**
- 15: **5. Physics-Informed Residuals**
- 16: $\Delta_1, \Delta_2, du_dx, N_u \leftarrow$ apply physics roles and DeepHPM model
- 17: **6. Q-Learning for PDE Weights**
- 18: $w1_state = \mathbb{E} \left[\left(\frac{\partial \hat{y}}{\partial t} \right)^2 \right]$
- 19: $w2_state = \mathbb{E} \left[\left(\frac{\partial^2 \hat{y}}{\partial t^2} \right)^2 \right]$
- 20: $w3_state = \mathbb{E} \left[\left(\frac{\partial \hat{y}}{\partial t} - \mathcal{N}_u \right)^2 \right]$
- 21: $w4_state = \mathbb{E} \left[\mathbb{I}(y = 0) \cdot \hat{y}^2 \right]$
- 22: reward = (previous_rmse - valid_rmse) \times 10
- 23: find different W_i using Q-learning agents
- 24: **7. PDE Loss & Broken-Device Constraint**
- 25: $\mathcal{L}_{\text{PDE}} \leftarrow w_1 \|\Delta_1\|^2 + w_2 \|\Delta_2\|^2 + w_3 \|\Delta_1 - N_u\|^2 + \mathbf{1}_{Y=0} \|\hat{Y}_{\text{seq}}[:, -1]\|^2$
- 26: **end if**
- 27: **return** $Y_{\text{seq}}[:, -1], \mathcal{L}_{\text{PDE}}, s, a, \log p$

3 Experimental Validation

3.1 Results and comparison on different datasets

3.1.1 Performance evaluation metrics

$$\text{MAE} = \frac{1}{N} \sum_{i=1}^N |\hat{y}_i - y_i|$$

$$\text{RMSE} = \sqrt{\frac{1}{N} \sum_{i=1}^N (\hat{y}_i - y_i)^2}$$

$$\text{Score} = \sum_{i=1}^N \left\{ \begin{array}{ll} e^{-\frac{e_i}{13}} - 1, & \text{if } e_i < 0 \\ e^{\frac{e_i}{10}} - 1, & \text{if } e_i \geq 0 \end{array} \right\}, \quad \text{where } e_i = y_i - \hat{y}_i$$

$$\text{MAPE} = \frac{100\%}{N} \sum_{i=1}^N \left| \frac{e_i}{y_i} \right|, \quad \text{where } e_i = y_i - \hat{y}_i$$

3.1.2 PRONOSTIA dataset

The PRONOSTIA (PHM2012) bearing dataset, introduced for the IEEE PHM-2012 Prognostics Challenge, provides run-to-failure records of deep-groove ball bearings. The dataset was collected from the PRONOSTIA experimental platform at FEMTO-ST laboratory in France which its case is presented in Figure 9. It contains 17 trials of complete experiments for training and eleven truncated runs whose hidden endpoints are used to evaluate RUL prediction. Each run records data from twin orthogonal accelerometers sampled at 25.6 kHz, a PT-100 temperature probe at 10 Hz, and speed-torque-force channels at 100 Hz, ensuring broadband coverage of fault frequencies. Since no artificial defects are introduced, the bearings degrade naturally, often exhibiting concurrent faults in balls, races, and cages. This results in highly realistic signals that reflect real-world failure modes. Additional details about operating conditions are summarized in Table 1, while Table 2 outlines the PRONOSTIA data proportions as defined by the PHM2012 challenge [33].

In the preprocessing pipeline, raw horizontal acceleration data from the FEMTO bearing dataset is transformed into spectrogram-based features, which captures critical frequency-domain characteristics which is conventional in time series datasets [34]. The proposed model has offered an exceptional performance on this dataset, and captured degradation trends across all bearings, even those with sparse degradation features or abrupt changes. It achieved superior accuracy compared to state-of-the-art methods.

Table 1: PRONOSTIA dataset: operating conditions and corresponding runs.

Condition	Speed (rpm)	Load (N)	Dataset runs
1	1800	4000	Bearing1_1–1_7
2	1650	4200	Bearing2_1–2_7
3	1500	5000	Bearing3_1–3_3

Table 2: PRONOSTIA data proportions.

Data sets	Condition 1	Condition 2	Condition 3
Learning set	Bearing1_1	Bearing2_1	Bearing3_1
	Bearing1_2	Bearing2_2	Bearing3_2
	Bearing1_3	Bearing2_3	Bearing3_3
Test set	Bearing1_4	Bearing2_4	–
	Bearing1_5	Bearing2_5	–
	Bearing1_6	Bearing2_6	–
	Bearing1_7	Bearing2_7	–

Table 3: Performance comparison on PRONOSTIA.

Model	Year	RMSE	MAE
MCNN [35]	2019	0.1987	0.1542
COT [36]	2022	0.1096	0.0769
TT-ConvLSTM [37]	2023	0.1090	0.0870
WTE-Trans [38]	2024	0.1100	0.0930
ILCANet [39]	2025	<u>0.0890</u>	<u>0.0670</u>
RGPD (Proposed)		0.0778	0.0634

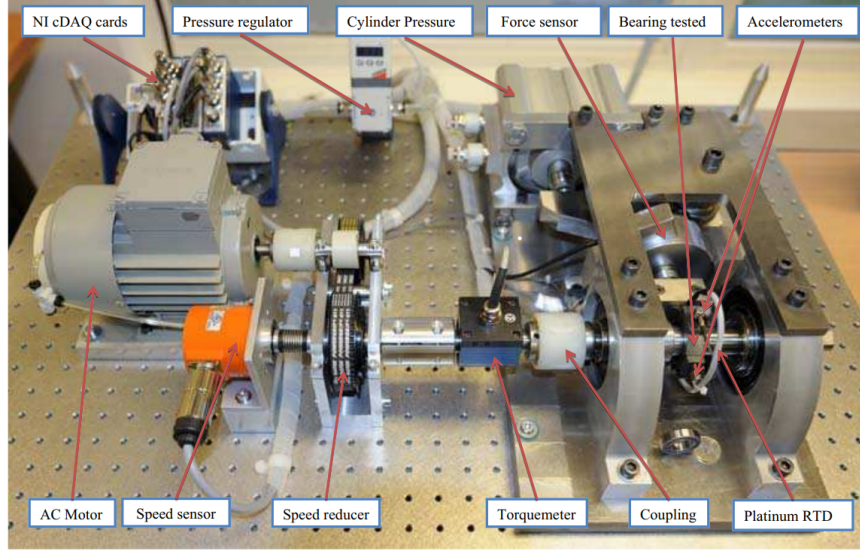


Figure 9: Overview of PRONOSTIA.

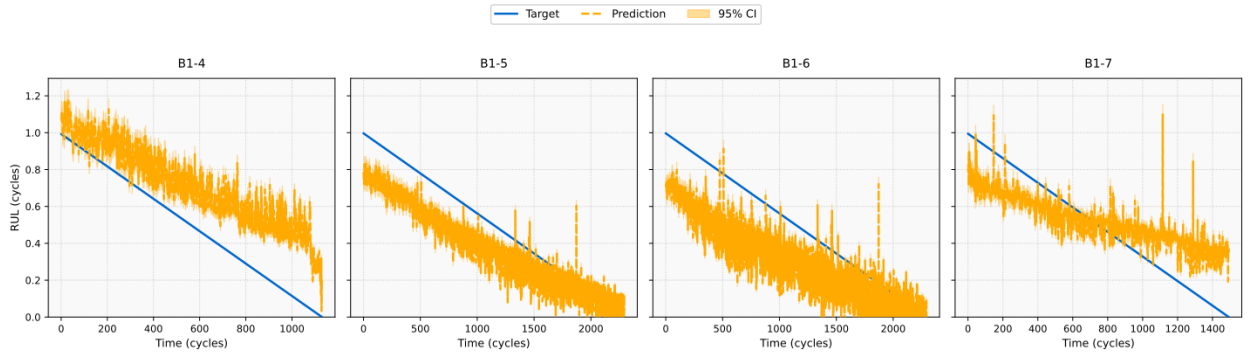


Figure 10: Prediction results with normalized targets of first condition bearings for PHM2012.

In Figure 10, results and predictions are plotted accordingly, we observe that predictions generally follow the trend of the targets, but some deviations are noticeable in B-7. In other bearings, even though there has been some deviations, the latest RUL predictions and targets are closely related, which is crucial for maintenance prognostics.

3.1.3 CMAPSS dataset

The C-MAPSS dataset serves as a simulated run-to-failure benchmark for engines. It contains 4 subsets (FD001–FD004) that differ by number of operating conditions and fault modes, and each subset provides a complete trajectories run to failure and test trajectories truncated before failure. At each cycle, three operational settings and 21 input channels are recorded, forming a rich multivariate time series. FD001 and FD003 simulate a single degradation mode under one operating condition, while FD002 and FD004 introduce six operating scenarios and two concurrent fault modes, increasing prognostic challenge complexity.

Thanks to its synthetic yet physics-based generation and standardized structure, C-MAPSS remains the prominent benchmark dataset for RUL estimation, underpinning hundreds of machine-learning studies and fostering reproducible comparisons across prognostic models. In Figure 11, the correlation matrices of CMAPSS subdatasets are depicted in a way that constant or less informative input channels are eliminated. It is clearly observed that FD002 and FD004, contain more informative input channels than FD001 and FD003. We employed a multi-time-window approach using three distinct window sizes for each sub-dataset, consistent with the method used by Li et al [40] and ZHOU et al [41] for data partitioning in RUL prediction.

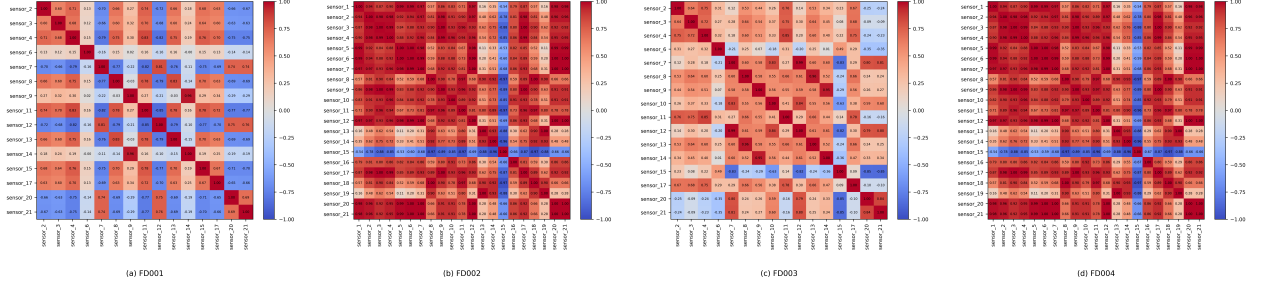


Figure 11: Correlation matrix of CMAPSS subdataset.

Figure 11 shows that FD001 and FD003 have generally lower correlations, indicating more independent channel behaviors, while FD002 and FD004 have stronger inter-channel correlations, suggesting complex operational conditions and possible redundancy, according to the heatmaps that show the linear relationships between input channel readings across the four CMAPSS subsets.

Table 4: Results comparison for CMPASS.

Model	Year	FD001		FD002		FD003		FD004		Average	
		RMSE	Score	RMSE	Score	RMSE	Score	RMSE	Score	RMSE	Score
Attention-LSTM [42]	2023	15.45	455.92	20.91	3602.94	14.67	473.97	24.01	6841.82	18.76	2843.66
ABGRU [13]	2023	12.83	221.54	17.97	2072.21	13.23	279.18	21.55	3625.77	16.39	1549.67
CATA-TCN [43]	2024	12.80	234.31	17.61	1361.23	13.16	290.63	21.04	2303.42	16.15	1047.40
BiGRU-TSAM [44]	2022	12.60	213.00	18.90	2264.00	12.50	233.00	20.50	3610.00	16.12	1580.00
MmoE-BiGRU [45]	2022	13.22	N/A	18.26	N/A	13.79	N/A	18.38	N/A	15.91	N/A
GAT-EdgePool [46]	2022	13.53	309.59	15.07	1380.41	14.66	470.74	17.60	1726.53	15.22	971.82
CNN-LSTM-SAM [47]	2023	12.60	261.00	15.30	1156.00	13.80	253.00	18.60	2425.00	15.08	1023.75
DA-TCN [48]	2021	11.78	229.48	16.95	1842.38	11.56	257.11	18.23	2317.32	14.63	1161.57
MTSTAN [49]	2023	<u>10.97</u>	175.36	16.81	1154.36	<u>10.90</u>	188.22	18.85	1446.20	14.38	741.53
GF-GGAT [16]	2025	11.71	<u>188.00</u>	14.92	990.47	13.06	<u>247.21</u>	15.71	<u>996.66</u>	13.85	<u>605.09</u>
PSTFormer [50]	2024	12.08	224.00	<u>13.00</u>	<u>877.00</u>	12.11	308.00	<u>14.38</u>	1182.00	<u>12.89</u>	647.75
AttnPINN [19]	2023	16.89	523	16.32	1479	17.75	1194	18.37	2059	17.33	1313.75
RGPD (Proposed)		10.77	207.09	11.58	684.24	10.78	245.28	12.38	787.39	11.38	481.00

The best results are **bolded**, and the second-best results are underlined.

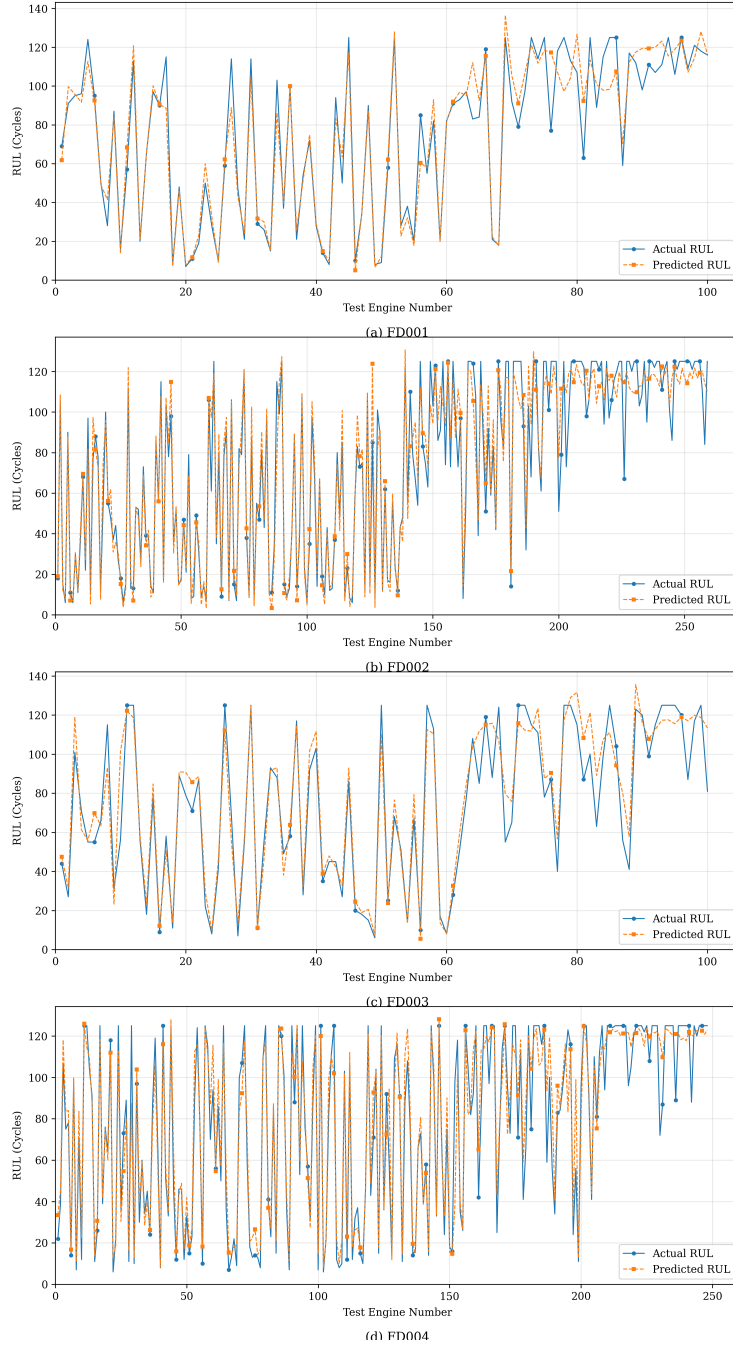


Figure 12: Prediction results with targets of total engines for each sub-data set of C-MAPSS.

In Figure 12, predictions alongside targets, are depicted and it demonstrates accurate engine RUL estimation, particularly in FD001, and FD003 which contain only 100 engines with fewer fault modes in comparison to FD002 and FD004 with more than 250 engines in each and higher fault modes.

As detailed in Table 4, the proposed model demonstrates exceptional performance in C-MAPSS dataset and sets a new standard for RUL prediction. It achieves superior accuracy and reliability, as evidenced by its minimized Root Mean Square Error (RMSE) and Score values across diverse operational contexts. The model's robustness is particularly notable in complex scenarios involving multiple operating conditions and fault modes, where it maintains precise and stable predictions. This consistency of excellence in various challenges underscores its generalizability and technical sophistication.

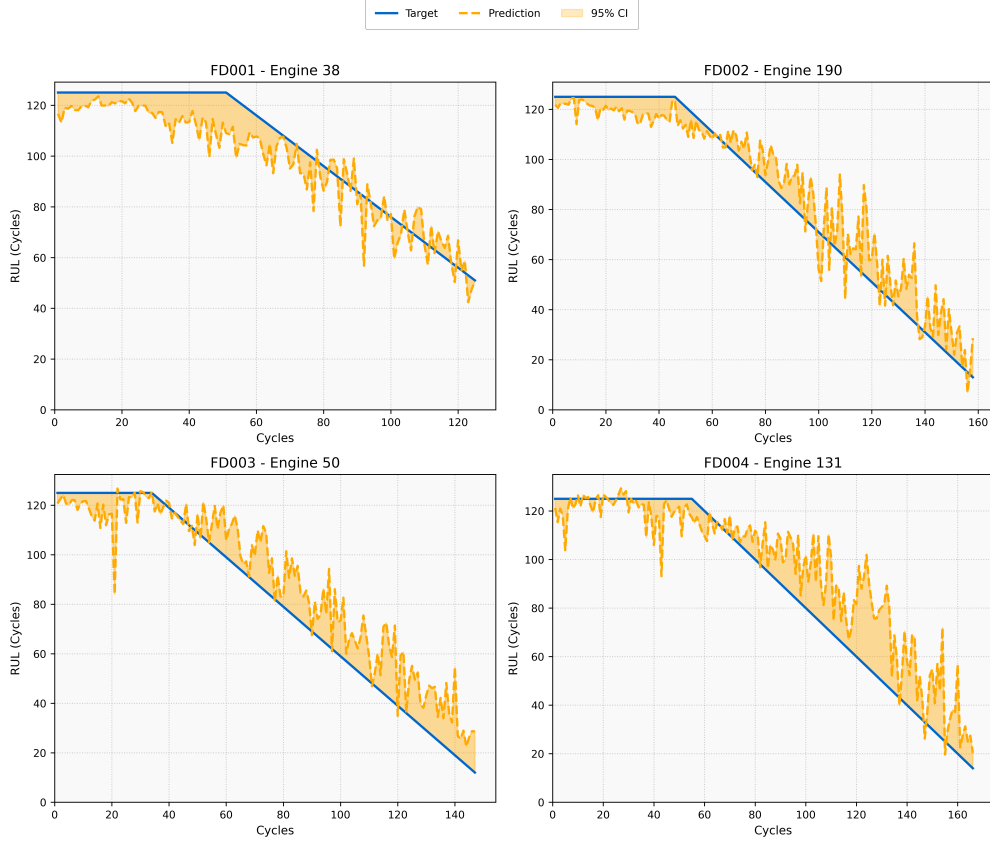


Figure 13: lifetime data of 4 random engines with targets and respective predictions of CMAPSS.

In addition to its robust performance, the proposed model introduces several key improvements that further enhance its capabilities. In particular, it achieves a significant reduction of 11.71% in average RMSE compared to the previous state-of-the-art, demonstrating a substantial leap in prediction accuracy. This is complemented by a 20.51% improvement in the average score metric, which indicates not only precise but also timely predictions.

Figure 13 shows RUL predictions for four random engines from the CMAPSS dataset. The model successfully captures the degradation trend, with predictions aligning well with the target. Importantly, the prediction accuracy significantly improves toward the end of the engine life, which is critical for reliable prognostics.

3.1.4 XJTU dataset

The dataset includes 55 lithium-ion batteries, tested under 6 different charging and discharging strategies. SOH estimation of the batteries is explicitly detailed with the proposed method and the model has proposed the best results of the data in many metrics.

As detailed in Table 5, the proposed model demonstrates superior performance in estimating the State-of-Health (SOH) of lithium-ion batteries on the XJTU dataset, particularly excelling in Mean Absolute Percentage Error (MAPE), a critical metric for battery health assessment due to its relative error interpretability. With an average MAPE of 0.86%, it outperforms Battery PINN (1.09%), MLP (2.52%), and CNN (2.88%), achieving lower MAPE in four out of six batches with improvements ranging from 0.20% to 0.48%. While its average Root Mean Square Error (RMSE) of 0.0105 is slightly higher than Battery PINN's 0.0085, it remains highly competitive, especially in key batches, highlighting its robustness. This consistent MAPE advantage, combined with competitive RMSE, positions the proposed model as a highly reliable and accurate solution for battery SOH estimation, enhancing its suitability for practical battery health monitoring applications.

Unlike the previous results, where the model's performance stood out clearly, the distinction here is less pronounced, suggesting only marginal improvements. Yet, the model has comprehensively maintained its performance in batteries as well as bearings and engines, which indicates its generalizability in diverse maintenance applications.

Figure 14 represents real SOH and prediction on time steps for different batches of the dataset, resulting in highly accurate predictions closely matching the real SOH. In comparison to PRONOSTIA and CMAPSS, XJTU’s predictions are more accurate due to lower noise and its unique feature interpretability.

Table 5: Batch-wise MAPE and RMSE comparison.

Method	Batch 1		Batch 2		Batch 3		Batch 4		Batch 5		Batch 6	
	RMSE	MAPE	RMSE	MAPE	RMSE	MAPE	RMSE	MAPE	RMSE	MAPE	RMSE	MAPE
MLP	0.0260	0.0277	0.0275	0.0304	0.0211	0.0237	0.0200	0.0235	0.0183	0.0217	0.0204	0.0242
CNN	0.0270	0.0330	0.0298	0.0352	0.0177	0.0212	0.0150	0.0189	0.0350	0.0453	0.0149	0.0194
Battery PINN [51]	0.0070	0.0094	0.0113	0.0122	0.0086	0.0100	0.0071	0.0105	0.0105	0.0135	0.0063	0.0097
RGPD (Proposed)	0.0055	0.0046	0.0100	0.0086	0.0093	0.0080	0.0134	0.0111	0.0180	0.0137	0.0070	0.0055

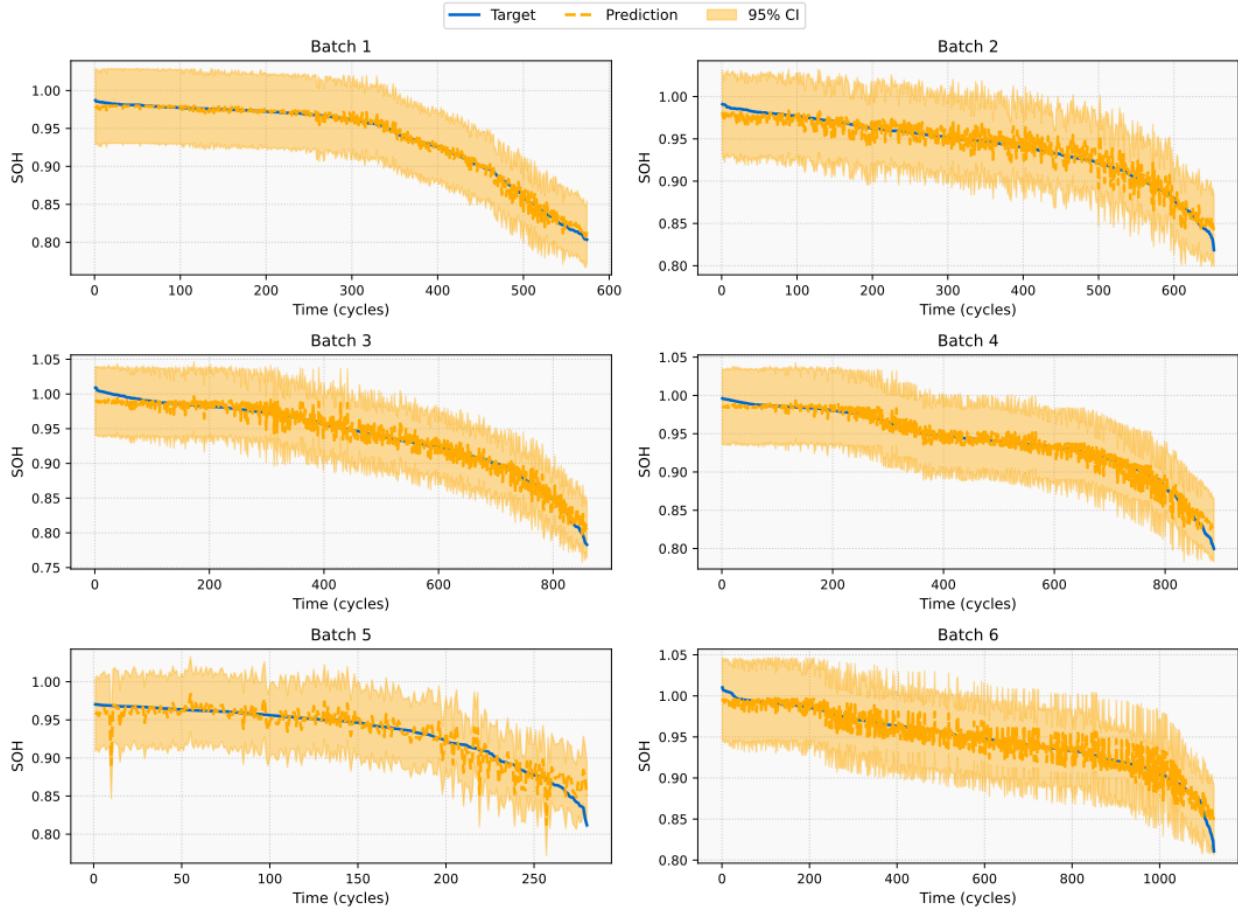


Figure 14: Prediction results alongside targets for different XJTU batches.

3.2 Physical constraint of different case studies

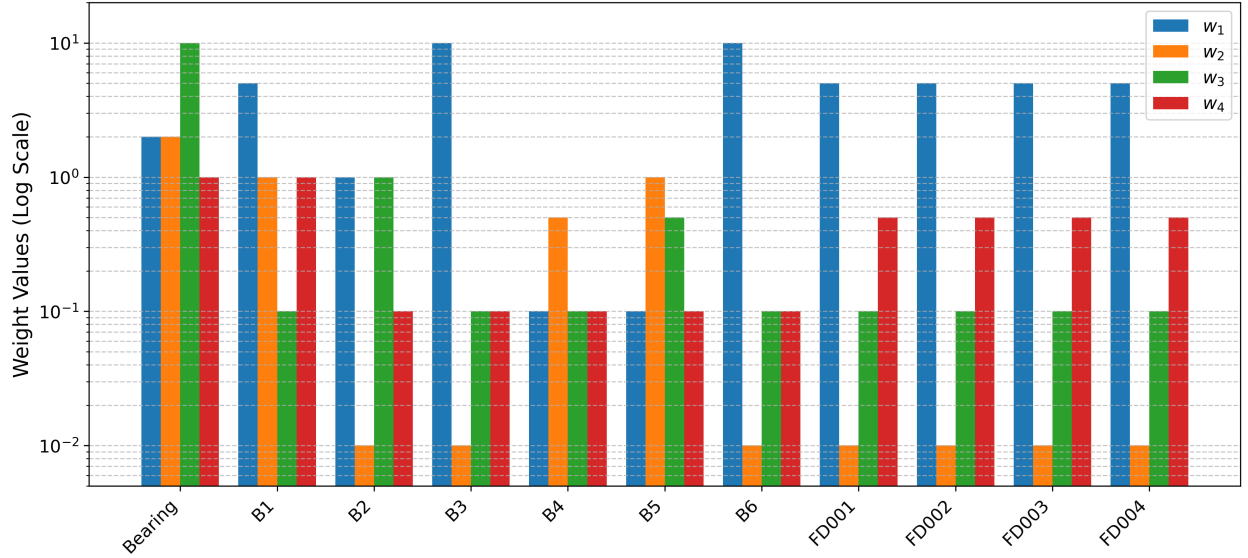


Figure 15: different learned weights for different industrial prognoses.

As shown in Figure 15, Q-learning agents have resulted in different weights for each physical constraint in different lifetime data from diverse applications. In CMAPSS sub-datasets, it led to identical weights for all of them, which indicates a solid connection between different physical constraints' importance and presence to obtain the most accurate results, particularly in CMAPSS dataset. In XJTU, this connection isn't as bold as CMAPSS yet, still we face a same trend between w3 and w4 for most of XJTU batches. Across various sub-datasets and applications, the decreasing RUL/SOH constraint (W_1) has consistently received greater emphasis than other constraints, and indicates its crucial role in accurate RUL and SOH estimation.

3.3 Visual feature contributions

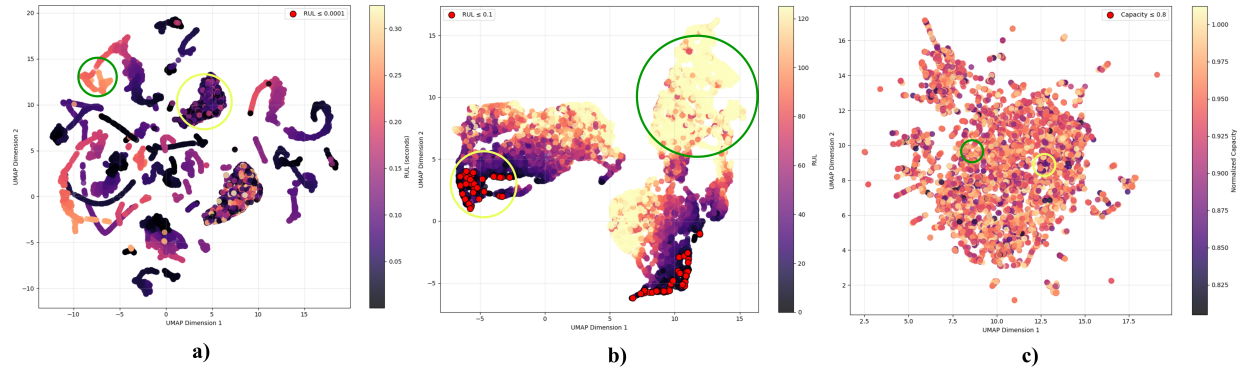


Figure 16: U-MAP feature mapping for diverse lifetime datasets of a) PRONOSTIA, b) CMAPSS, and c) XJTU. Green circle corresponds to healthy state and yellow circle corresponds to final degradation states of the devices.

As shown in Figure 16, panel (a) presents scattered degradation paths with distinct low-RUL clusters, highlighting varied failure modes. This is reasonably caused due to presence of bearings with different operating conditions in the evaluated dataset. In panel (b), there is a clearer separation between healthy and degraded regions, and indicates stronger RUL progression structures, because of the characterized and detailed features in long sequences of CMAPSS. panel (c), presents a dense, less structured SOH space with subtle degradation patterns and weaker separability due

to the critical difference of SOH and RUL, which the battery still has maintained at least 80% of its initial capacity in the end of its lifetime, so the features are mapped in a more overlapping state than RUL prediction.

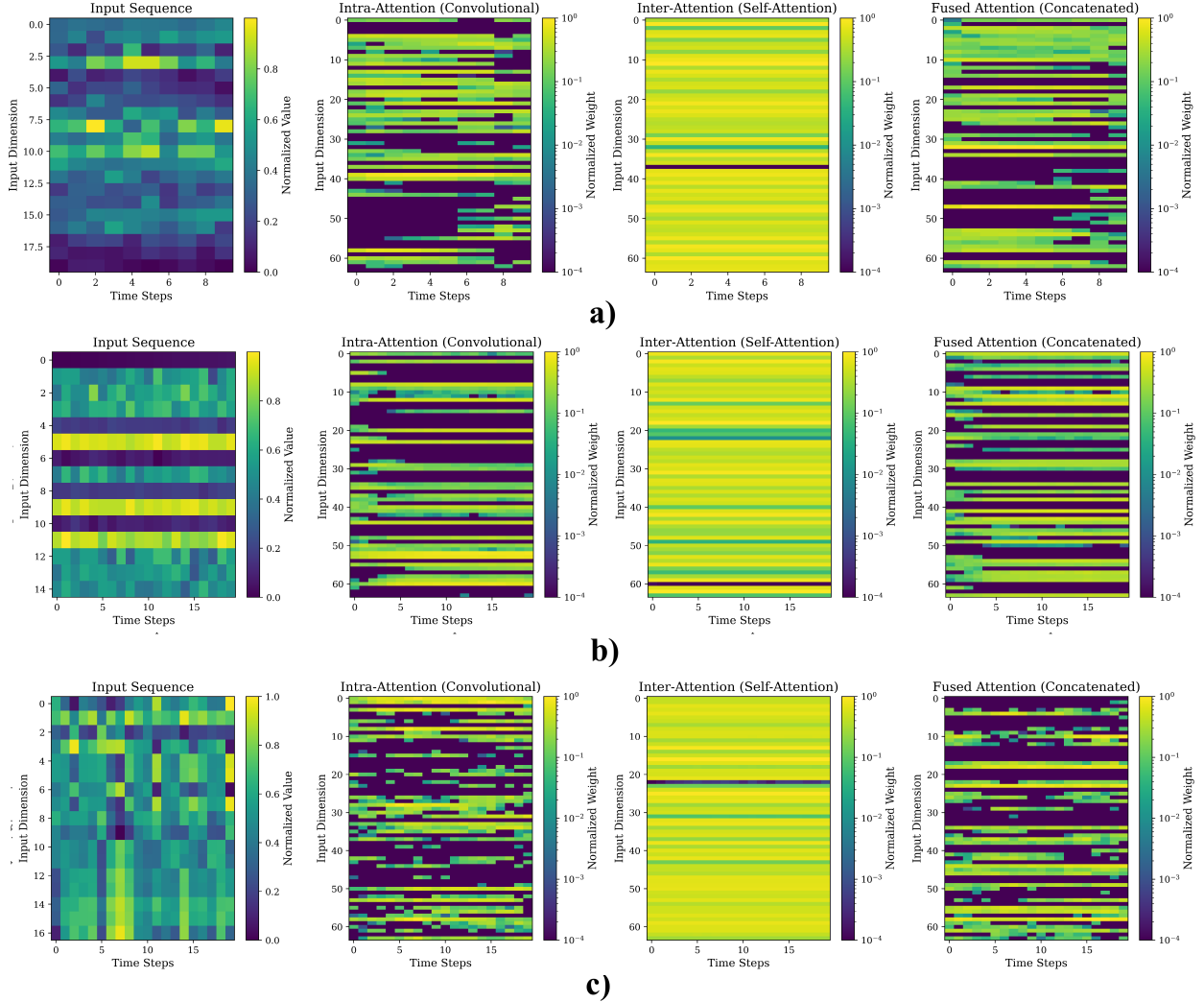


Figure 17: The comparison of input sequences, Intra-attention output, inter-attention output and their concatenation as resulted weights for a)PRONOSTIA, b)XJTU, and c)CMAPSS.

Figure 17 presents attention visualizations for three input samples using intra-attention (convolutional), inter-attention (self-attention), and fused attention mechanisms. The input sequence heatmaps show distinct temporal and dimensional patterns across samples. Intra-attention emphasizes localized feature dependencies with sparse, high-contrast weights. Inter-attention distributes focus more evenly and captures global temporal relationships. Collectively, fused attention integrates both local and global insights for richer representations.

3.4 Ablation Study

For better understanding of the effect of each component, we also test the model when it is absent.

Table 6: Performance metrics of ablation models on PHM2012.

Model	RMSE	MAE
Complete model	0.0778	0.0634
Without RL	0.0923	0.0775
With Mixup	0.0986	0.0830
Without TAU	0.0818	0.0681

Table 7: Performance metrics of ablation models on C-MAPSS subsets.

Model	FD001		FD002		FD003		FD004	
	RMSE	Score	RMSE	Score	RMSE	Score	RMSE	Score
Complete model	10.771	207.09	11.58	684.24	10.785	245.28	12.381	787.39
Without RL	11.556	290.15	11.477	653.07	10.804	274.41	12.630	781.30
Without Mixup	12.005	266.51	11.466	616.79	11.237	299.77	11.973	723.29
Without TAU	12.334	320.10	12.209	851.67	11.092	311.25	13.031	904.63

Table 8: Performance metrics of ablation models on different batches of XJTU.

Model	Batch1			Batch2			Batch3			Batch4			Batch5			Batch6		
	RMSE	MAPE	MAE	RMSE	MAPE	MAE	RMSE	MAPE	MAE	RMSE	MAPE	MAE	RMSE	MAPE	MAE	RMSE	MAPE	MAE
Complete model	0.0055	0.46%	0.0043	0.0100	0.86%	0.0080	0.0093	0.80%	0.0074	0.0134	1.11%	0.0103	0.0180	1.37%	0.0126	0.0070	0.55%	0.0052
Without RL	0.0057	0.46%	0.0041	0.0069	0.56%	0.0052	0.0096	0.81%	0.0074	0.0103	0.85%	0.0079	0.0117	0.93%	0.0085	0.0112	0.98%	0.0091
With Mixup	0.0080	0.67%	0.0062	0.0162	1.37%	0.0129	0.0299	2.55%	0.0235	0.0179	1.46%	0.0136	0.0158	1.24%	0.0114	0.0125	0.99%	0.0093
Without TAU	0.0568	6.05%	0.0564	0.0212	1.84%	0.0170	0.2896	30.88%	0.2894	0.1365	10.33%	0.0987	0.0884	9.42%	0.0877	0.0084	0.73%	0.0069

In this section, we ablated some components and created three cases: removing RL agents, Mixup data augmentation, and the TAU block. Each ablation helps isolate the contribution of individual modules to the overall model performance. In Table 6, Table 7, and Table 8 the ablation results from PRONOSTIA, CMAPSS, and XJTU are listed respectively.

3.4.1 Reinforcement Learning Role

The model can adaptively assign weights to the physics-informed loss terms and dynamically scale hidden representations, thanks to the RL modules, especially the Q-learning agents. This dynamic adjustment is essential for striking a balance between physical consistency and empirical data fitting, and led to higher accuracy and generalization, particularly when working with diverse datasets that have different degradation dynamics.

Upon removal of RL, the model exhibits a consistent deterioration in predictive accuracy, as evidenced by increased RMSE and MAE across all datasets. On the C-MAPSS benchmark dataset, the score and error metrics rise notably in FD001 and FD003 subsets, which contain more consistent degradation patterns. The same trend was observed in PRONOSTIA dataset with different operational conditions, which suggests that RL helps the model generalize well across varying operational conditions and prevents overfitting to specific patterns.

Furthermore, although reinforcement learning (RL) is useful on complex datasets such as CMAPSS, where it improves performance by allowing adaptive learning in real-time, noisy industrial environments with less deterministic patterns, it might not always be advantageous. Because XJTU is small and relatively simple, RL has a tendency to overfit, which results in a slight decrease in accuracy. Consequently, our suggested model without RL performs better in the majority of situations, even though RL is optimal in roughly half of them. This implies that leaving out RL can produce better outcomes when working with small or simpler datasets. Our suggested model performs the best on average in every scenario.

3.4.2 Mixup Regularization Role

In the CMAPSS dataset, applying mixup between FD001 and FD003 can lead to improved evaluation metrics. However, for FD002 and FD004, where the data is more complex and sensitive, linear data mixing and synthetic data generation may result in increased RMSE and a drop in performance. Similarly, in the XJTU and PRONOSTIA datasets, due to the limited number of sequences compared to CMAPSS, mixup does not provide noticeable improvements in prediction accuracy and is therefore not used in the base model.

3.4.3 Temporal Attention Unit Role

In this section, we replaced the TAU blocks of the model with simple multi-head attention layers. As evident from the tables, among the components analyzed, TAU proves to be the most impactful for maintaining predictive accuracy. It enables the model to focus on spatio-temporal features, and dynamically adjusts the weight of past observations in recurrent processing. This capability is crucial for modeling global and local dependencies in degradation sequences.

The removal of TAU results in the steepest decline in performance across all datasets. In C-MAPSS, models without TAU perform worst on all four subsets, with FD004 suffering the most — likely due to its longer sequences and higher variance in operating conditions.

In the XJTU dataset, the ablation of TAU leads to dramatic increases in RMSE and MAE, particularly in Batch4 and Batch6. These results affirm that TAU is essential for tracking gradual and non-linear degradation, especially where degradation signals are weak or noisy. Without it, the model struggles to discriminate between informative and redundant signals, that leads to predictions with lower accuracy.

4 Conclusion

This study introduced a reinforced graph-based physics-informed neural network PINN framework that synergistically combines temporal attention mechanisms, graph convolutional architectures, and reinforcement learning strategies to estimate RUL and SOH in industrial systems. By integrating modules such as TAU and GATConv, the model adeptly captures complex spatio-temporal dependencies inherent in degradation data. The incorporation of reinforcement learning techniques, specifically Q-learning and SAC, facilitates dynamic adjustment of physics-based loss weights and adaptive scaling of hidden representations, enhancing the model’s adaptability across diverse datasets.

Empirical evaluations on benchmark datasets—PRONOSTIA, CMAPSS, and XJTU—demonstrated the model’s superior performance compared to existing state-of-the-art methods. The ablation studies underscored the individual contributions of each component, affirming the efficacy of the integrated approach.

While the proposed framework exhibits robust performance, certain limitations warrant consideration. The reliance on specific benchmark datasets may not fully encapsulate the variability present in all real-world scenarios.

Future research directions include exploring the model’s applicability to a broader range of industrial systems and degradation patterns, optimizing computational efficiency for real-time applications, and integrating additional data modalities to further enhance predictive accuracy and generalizability.

References

- [1] Yang Hu, Xuewen Miao, Yong Si, Ershun Pan, and Enrico Zio. Prognostics and health management: A review from the perspectives of design, development and decision. *Reliability Engineering & System Safety*, 217:108063, 2022.
- [2] Yaguo Lei, Naipeng Li, Liang Guo, Ningbo Li, Tao Yan, and Jing Lin. Machinery health prognostics: A systematic review from data acquisition to rul prediction. *Mechanical Systems and Signal Processing*, 104:799–834, 2018.
- [3] Lei Wang, Zhiwen Liu, Hongrui Cao, and Xin Zhang. Subband averaging kurtogram with dual-tree complex wavelet packet transform for rotating machinery fault diagnosis. *Mechanical Systems and Signal Processing*, 142:106755, 2020.
- [4] Behnoush Rezaeianjouybari and Yi Shang. Deep learning for prognostics and health management: State of the art, challenges, and opportunities. *Measurement*, 163:107929, 2020.
- [5] Tiago Zonta, Cristiano André da Costa, Rodrigo da Rosa Righi, Miromar José de Lima, Eduardo Silveira da Trindade, and Guann Pyng Li. Predictive maintenance in the industry 4.0: A systematic literature review. *Computers & Industrial Engineering*, 150:106889, 2020.

- [6] Huiqin Li, Zhengxin Zhang, Tianmei Li, and Xiaosheng Si. A review on physics-informed data-driven remaining useful life prediction: Challenges and opportunities. *Mechanical Systems and Signal Processing*, 209:111120, 2024.
- [7] F. Wang, Z. Zhai, Z. Zhao, et al. Physics-informed neural network for lithium-ion battery degradation stable modeling and prognosis. *Nature Communications*, 15:4332, 2024.
- [8] Tianzhi Li, Jian Chen, Shenfang Yuan, Francesco Cadini, and Claudio Sbarufatti. Particle filter-based damage prognosis using online feature fusion and selection. *Mechanical Systems and Signal Processing*, 203:110713, 2023.
- [9] May Htet Htet Khine, Cheong Ghil Kim, and Nattapol Aunsri. A review of bayesian-filtering-based techniques in rul prediction for lithium-ion batteries. *Journal of Energy Storage*, 111:115371, 2025.
- [10] Kedar Kirane and Zdeněk P. Bažant. Size effect in paris law and fatigue lifetimes for quasibrittle materials: Modified theory, experiments and micro-modeling. *International Journal of Fatigue*, 83:209–220, 2016.
- [11] Liang Guo, Naipeng Li, Feng Jia, Yaguo Lei, and Jing Lin. A recurrent neural network based health indicator for remaining useful life prediction of bearings. *Neurocomputing*, 240:98–109, 2017.
- [12] Ibomoiye Domor Mienye, Theo G. Swart, and George Obaido. Recurrent neural networks: A comprehensive review of architectures, variants, and applications. *Information*, 15(9), 2024.
- [13] Ruiguan Lin, Huawei Wang, Minglan Xiong, Zhaoguo Hou, and Changchang Che. Attention-based gate recurrent unit for remaining useful life prediction in prognostics. *Applied Soft Computing*, 143:110419, 2023.
- [14] Han Li, Wei Zhao, Yuxi Zhang, and Enrico Zio. Remaining useful life prediction using multi-scale deep convolutional neural network. *Applied Soft Computing*, 89:106113, 2020.
- [15] Yucheng Wang, Min Wu, Xiaoli Li, Lihua Xie, and Zhenghua Chen. A survey on graph neural networks for remaining useful life prediction: Methodologies, evaluation and future trends. *Mechanical Systems and Signal Processing*, 229:112449, 2025.
- [16] Yu Wang, Shangjing Peng, Hong Wang, Mingquan Zhang, Hongrui Cao, and Liwei Ma. Remaining useful life prediction based on graph feature attention networks with missing multi-sensor features. *Reliability Engineering & System Safety*, 258:110902, 2025.
- [17] Alejandro Barredo Arrieta, Natalia Díaz-Rodríguez, Javier Del Ser, Adrien Bannetot, Siham Tabik, Alberto Barbado, Salvador Garcia, Sergio Gil-Lopez, Daniel Molina, Richard Benjamins, Raja Chatila, and Francisco Herrera. Explainable artificial intelligence (xai): Concepts, taxonomies, opportunities and challenges toward responsible ai. *Information Fusion*, 58:82–115, 2020.
- [18] M. Raissi, P. Perdikaris, and G.E. Karniadakis. Physics-informed neural networks: A deep learning framework for solving forward and inverse problems involving nonlinear partial differential equations. *Journal of Computational Physics*, 378:686–707, 2019.
- [19] Xinyuan Liao, Shaowei Chen, Pengfei Wen, and Shuai Zhao. Remaining useful life with self-attention assisted physics-informed neural network. *Advanced Engineering Informatics*, 58:102195, 2023.
- [20] Yapeng Zhou and Miaohua Huang. Lithium-ion batteries remaining useful life prediction based on a mixture of empirical mode decomposition and arima model. *Microelectronics Reliability*, 65:265–273, 2016.
- [21] Ashish Kumar Shakya, Gopinatha Pillai, and Sohom Chakrabarty. Reinforcement learning algorithms: A brief survey. *Expert Systems with Applications*, 231:120495, 2023.
- [22] Erotokritos Skordilis and Ramin Moghaddass. A deep reinforcement learning approach for real-time sensor-driven decision making and predictive analytics. *Computers & Industrial Engineering*, 147:106600, 2020.
- [23] Changgang Zheng, Shufan Yang, Juan Parra-Ullauri, Antonio Garcia-Dominguez, and Nelly Bencomo. Reward-reinforced reinforcement learning for multi-agent systems, 2021.
- [24] Cheng Liu, Yan Chen, and Xuebing Xu. Fatigue life prognosis of composite structures using a transferable deep reinforcement learning-based approach. *Composite Structures*, 353:118727, 2025.
- [25] Cheng Tan, Zhangyang Gao, Lirong Wu, Yongjie Xu, Jun Xia, Siyuan Li, and Stan Z. Li. Temporal attention unit: Towards efficient spatiotemporal predictive learning. In *2023 IEEE/CVF Conference on Computer Vision and Pattern Recognition (CVPR)*, pages 18770–18782, 2023.
- [26] Yixiang Lu, Daiqi Tang, De Zhu, Qingwei Gao, Dawei Zhao, and Junwen Lyu. Remaining useful life prediction for bearing based on coupled diffusion process and temporal attention. *IEEE Transactions on Instrumentation and Measurement*, 73:1–10, 2024.
- [27] Thomas N. Kipf and Max Welling. Semi-supervised classification with graph convolutional networks, 2017.

- [28] Jinglong Chen, Hongjie Jing, Yuanhong Chang, and Qian Liu. Gated recurrent unit based recurrent neural network for remaining useful life prediction of nonlinear deterioration process. *Reliability Engineering & System Safety*, 185:372–382, 2019.
- [29] Maziar Raissi. Deep hidden physics models: Deep learning of nonlinear partial differential equations, 2018.
- [30] Christopher J.C.H. Watkins and Peter Dayan. Q-learning. *Machine Learning*, 8(3):279–292, 1992.
- [31] Tuomas Haarnoja, Aurick Zhou, Pieter Abbeel, and Sergey Levine. Soft actor-critic: Off-policy maximum entropy deep reinforcement learning with a stochastic actor, 2018.
- [32] Hongyi Zhang, Moustapha Cisse, Yann N. Dauphin, and David Lopez-Paz. mixup: Beyond empirical risk minimization, 2018.
- [33] Patrick Nectoux, Rafael Gouriveau, Kamal Medjaher, Emmanuel Ramasso, Brigitte Chebel-Morello, Nathalie Zerhouni, and Christophe Varnier. PRONOSTIA: An experimental platform for bearings accelerated degradation tests. In *IEEE International Conference on Prognostics and Health Management (PHM)*, pages 1–8, Denver, Colorado, United States, June 2012. IEEE.
- [34] Juan Antonio Cortés-Ibáñez, Sergio González, José Javier Valle-Alonso, Julián Luengo, Salvador García, and Francisco Herrera. Preprocessing methodology for time series: An industrial world application case study. *Information Sciences*, 514:385–401, 2020.
- [35] Jun Zhu, Nan Chen, and Weiwen Peng. Estimation of bearing remaining useful life based on multiscale convolutional neural network. *IEEE Transactions on Industrial Electronics*, 66(4):3208–3216, 2019.
- [36] Yifei Ding and Mingping Jia. Convolutional transformer: An enhanced attention mechanism architecture for remaining useful life estimation of bearings. *IEEE Transactions on Instrumentation and Measurement*, 71:1–10, 2022.
- [37] Sajawal Gul Niazi, Tudi Huang, Hongming Zhou, Song Bai, and Hong-Zhong Huang. Multi-scale time series analysis using tt-convlstm technique for bearing remaining useful life prediction. *Mechanical Systems and Signal Processing*, 206:110888, 2024.
- [38] Wenhao Zou, Zhiqiang Lu, Zhiyong Hu, and Lei Mao. Remaining useful life estimation of bearing using deep multiscale window-based transformer. *IEEE Transactions on Instrumentation and Measurement*, 72:1–11, 2023.
- [39] Mingyuan Zhang, Chen He, Chengxuan Huang, and Jianhong Yang. A weighted time embedding transformer network for remaining useful life prediction of rolling bearing. *Reliability Engineering & System Safety*, 251:110399, 2024.
- [40] H. Li, P. Cao, X. Wang, B. Yi, M. Huang, Q. Sun, and Y. Zhang. Multi-task spatio-temporal augmented net for industry equipment remaining useful life prediction. *Advanced Engineering Informatics*, 55:101898, 2023.
- [41] Di ZHOU, Xiao ZHUANG, and Hongfu ZUO. A hybrid deep neural network based on multi-time window convolutional bidirectional lstm for civil aircraft apu hazard identification. *Chinese Journal of Aeronautics*, 35(4):344–361, 2022.
- [42] Xianzhe Cheng, Kehong Lv, Yong Zhang, Lei Wang, Weihua Zhao, Guanjun Liu, and Jing Qiu. Rul prediction method for electrical connectors with intermittent faults based on an attention-lstm model. *IEEE Transactions on Components, Packaging and Manufacturing Technology*, 13(5):628–637, 2023.
- [43] Lin Lin, Jinlei Wu, Song Fu, Sihao Zhang, Changsheng Tong, and Lizheng Zu. Channel attention & temporal attention based temporal convolutional network: A dual attention framework for remaining useful life prediction of the aircraft engines. *Advanced Engineering Informatics*, 60:102372, 2024.
- [44] Jiushi Zhang, Yuchen Jiang, Shimeng Wu, Xiang Li, Hao Luo, and Shen Yin. Prediction of remaining useful life based on bidirectional gated recurrent unit with temporal self-attention mechanism. *Reliability Engineering & System Safety*, 221:108297, 2022.
- [45] Yong Zhang, Yuqi Xin, Zhi wei Liu, Ming Chi, and Guijun Ma. Health status assessment and remaining useful life prediction of aero-engine based on bigru and mmoe. *Reliability Engineering & System Safety*, 220:108263, 2022.
- [46] Tianfu Li, Zheng Zhou, Sinan Li, Chuang Sun, Ruqiang Yan, and Xuefeng Chen. The emerging graph neural networks for intelligent fault diagnostics and prognostics: A guideline and a benchmark study. *Mechanical Systems and Signal Processing*, 168:108653, 2022.
- [47] Jie Li, Yuanjie Jia, Mingbo Niu, Wei Zhu, and Fanxi Meng. Remaining useful life prediction of turbofan engines using cnn-lstm-sam approach. *IEEE Sensors Journal*, 23(9):10241–10251, 2023.
- [48] Yan Song, Shengyao Gao, Yibin Li, Lei Jia, Qiqiang Li, and Fuzhen Pang. Distributed attention-based temporal convolutional network for remaining useful life prediction. *IEEE Internet of Things Journal*, 8(12):9594–9602, 2021.

- [49] Haodong Li, Peng Cao, Xingwei Wang, Bo Yi, Min Huang, Qiuye Sun, and Yanfeng Zhang. Multi-task spatio-temporal augmented net for industry equipment remaining useful life prediction. *Advanced Engineering Informatics*, 55:101898, 2023.
- [50] Song Fu, Yiming Jia, Lin Lin, Shiwei Suo, Feng Guo, Sihao Zhang, and Yikun Liu. Pstformer: A novel parallel spatial-temporal transformer for remaining useful life prediction of aeroengine. *Expert Systems with Applications*, 265:125995, 2025.
- [51] Fujin Wang, Zhi Zhai, Zhibin Zhao, Yi Di, and Xuefeng Chen. Physics-informed neural network for lithium-ion battery degradation stable modeling and prognosis. *Nature Communications*, 15(1):4332, 2024.